

# Optimisation of the enamelling of an apatite–mullite glass–ceramic coating on $\text{Ti}_6\text{Al}_4\text{V}$

Kevin P. O’Flynn · Kenneth T. Stanton

Received: 14 February 2011 / Accepted: 9 July 2011 / Published online: 20 July 2011  
© Springer Science+Business Media, LLC 2011

**Abstract** Apatite–mullite glass–ceramics (AMGCs) are under investigation as a potential alternative to hydroxyapatite (HA) as a coating for cementless fixation of orthopaedic implants. These materials have tailorable mechanical and chemical properties that make them attractive for use as bioactive coatings. Here, AMGC coatings on  $\text{Ti}_6\text{Al}_4\text{V}$  were investigated to determine an improved heat treatment regime using a systematic examination of the different inputs: composition of glass, nucleation hold and crystallisation hold. An upper limit to the heat treatment temperature was determined by the  $\alpha + \beta \rightarrow \beta$  of  $\text{Ti}_6\text{Al}_4\text{V}$  at  $970^\circ\text{C}$ . The glass composition was modified to produce different crystallisation temperatures and sintering characteristics. A glass was found that is fully crystalline below  $970^\circ\text{C}$  and has good sinterability. The effects of different heat treatment time and temperature combinations on the coating and substrate morphologies were examined and the most suitable combination determined. This sample was further investigated and was found to have qualitatively good adhesion and evidence of an interfacial reaction region between the coating and substrate indicating that a chemical reaction had occurred. Oxygen infiltration into the substrate was quantified and the new route was shown to result in a 63% reduction in penetration depth.

## 1 Introduction

Cementless fixation of biomedical implants is now feasible in a variety of different applications and their designs have now shown medium- and long-term success comparable to that of cemented fixation [6]. A prospective analysis of 1,000 patients with cementless, hydroxyapatite (HA)-coated total knee replacements showed a cumulative survival at 10 years of 99.14% with revision as the end point [6]. A separate study showed 97.5% survival at 12 years in 118 HA-coated cementless total knee replacements in young (<55 years of age) patients with primary or post-traumatic osteoarthritis [27]. Cementless fixation is also successfully used in acetabular shell revisions resulting in survivorship of 95% at 20 years with the end point as revision for aseptic loosening or radiographic evidence of loosening [20]. Cementless implants are often coated with synthetic HA [ $\text{Ca}_{10}(\text{PO}_4)_6(\text{OH})_2$ ] to enhance osseointegration. This is done typically by either plasma spraying or sintering but both routes cause different problems. Plasma spraying produces a mixed crystallinity coating with amorphous and crystalline phases which can result in mixed dissolution rates [10]. High temperature sintering can cause inadequate strength in the coating and the dehydroxylation of the HA [5].

Glass–ceramics offer an alternative to synthetic HA. Calcium-phosphate based glasses and glass–ceramics have demonstrated great potential for use in vivo because their chemical composition resembles that of HA [13]. They can be produced with little or no porosity, have a reproducible fine-grained microstructure [19] and can have mechanical and biological properties tailored to specific applications [8, 22]. Here, we use apatite–mullite glass–ceramics (AMGCs), which crystallize to form fluorapatite (FAP,  $\text{Ca}_{10}(\text{PO}_4)_6\text{F}_2$ ) and mullite ( $\text{Si}_2\text{Al}_6\text{O}_{13}$ ) [26]. FAP is a

---

K. P. O’Flynn · K. T. Stanton (✉)  
School of Mechanical and Materials Engineering,  
University College Dublin, Belfield, Dublin 4, Ireland  
e-mail: kenneth.stanton@ucd.ie

fluorine analogue of the HA found in human teeth and bone [4]. It is more stable than HA and has a lower bioresorption rate [12]. Mullite is an inert phase and gives the material excellent mechanical strength. AMGCs have been shown to be osseoconductive in vivo [8].

When used as a coating material, it has been demonstrated that AMGCs can be successfully deposited as a glass on titanium alloy substrates and enamelled in situ [23–25]. This method combines the reactivity of a glass during processing with the stability of a ceramic when fully cerammed. In a previous examination into the bonding of AMGCs to titanium alloys, the coating interface was examined using transmission electron microscopy (TEM) to determine the nature of the reactions occurring during bonding [24, 25]. The interface is a complex reaction region and the formation of titanium silicides and titanium phosphides were observed as interfacial reaction products in addition to significant grain growth occurring in the substrate [23]. While it has been proven that glass-ceramics can be successfully enamelled to titanium substrates [23], little analysis has been presented to determine an optimised route or to control the coating morphology.

This paper attempts to systematically examine a number of factors affecting the resultant coating and define an improved heat treatment protocol. A suitable coating surface would have sufficient mechanical integrity and provide a surface that encourages cell proliferation. Deligianni et al. [7] have shown that “surface roughness of HA generally improved the short- and longer-term response of bone marrow cells in vitro” and Bigerelle et al. [2] determined that a topology “formed by many bowl-like nests favouring cell adhesion and growth” for Ti surfaces.

The titanium alloy  $Ti_6Al_4V$  is known as a high-temperature alloy, making it is suitable for use with an enamelling route. However there are limits to the enamelling temperature. Sha and Guo [21] investigated the solid state transformation of  $Ti_6Al_4V$  under continuous heating and found that little change occurs in the material below 970°C. The only change that did occur was a  $\beta \rightarrow \beta$  where the  $\beta$  phase transformed into a high temperature  $\beta$  phase. They also observed the formation of Widmanstätten when the sample was heated to 1,000°C. They point out that at, and above, this

temperature “in most cases  $\alpha + \beta \rightarrow \beta$  transformation in  $\alpha + \beta$  titanium alloys develops via the increase of  $\beta$  phase volume, because of migration of  $\alpha/\beta$  interface” [21]. Therefore, it is sensible to impose an upper limit of 970°C as the maximum permissible sintering temperature so as to avoid a phase change in the substrate. The role of alloying elements Al and V in changing the alloy transus temperature is described in detail by Long and Rack [16].

## 2 Materials and methods

### 2.1 Glass synthesis

A FAP–mullite glass–ceramic system was used with the composition  $1.5(5 - x_F)SiO_2 - (5 - x_F)Al_2O_3 - 1.5P_2O_5 - (5 - x_F)CaO - x_FCaF_2$ , where  $x_F$  can vary between 1.0 and 2.5. The glass codes corresponding to the different  $x_F$  values are given in Table 1. This glass series was chosen as it has been designed to maintain an apatitic Ca:P ratio of 1.67 [25]. The reagents were mixed for 40 min in a ball mill without  $P_2O_5$  due to the hygroscopic nature of the latter component. The  $P_2O_5$  was then added and the mixture ball-milled for a further 15 min. The powder was then placed into a high density lidded mullite crucible. Using an electric furnace, the crucible and charge were heated to the required firing temperature (see Table 1) and held at this temperature for 1 h. The glass melt was then poured directly into demineralised water to shock quench to room temperature, thereby avoiding crystallization and preserving the amorphous nature of the glass. The glass was dried in an oven at 70°C for 1 day, then crushed and sieved to produce powders with particle sizes of <45  $\mu m$ , >45  $\mu m$  and <125  $\mu m$  and >125  $\mu m$ , referred to as fine, coarse and frit respectively.

### 2.2 Differential scanning calorimetry (DSC)

Thermal analysis was performed using a Rheometric Scientific STA 1600 (Surrey, UK). The glasses were placed in matched platinum-rhodium crucibles in a flowing dry nitrogen atmosphere with a heating rate of 10 K min<sup>-1</sup>.

**Table 1** Glasses used with codes,  $x_F$  values and components by wt%

Glass code	G250	G220	G200	G187	G175	G150	G125	G100
$x_F$ value	2.50	2.20	2.00	1.87	1.75	1.50	1.25	1.00
SiO <sub>2</sub> (wt%)	21.91	23.38	24.28	24.84	25.34	26.32	27.23	28.08
Al <sub>2</sub> O <sub>3</sub> (wt%)	24.78	26.45	27.47	28.10	28.66	29.77	30.81	31.77
P <sub>2</sub> O <sub>5</sub> (wt%)	20.70	19.72	19.12	18.75	18.42	17.76	17.16	16.59
CaF <sub>2</sub> (wt%)	18.98	15.91	14.02	12.86	11.82	9.77	7.86	6.08
CaO (wt%)	13.63	14.54	15.11	15.46	15.76	16.37	16.94	17.47

DSC analysis of three different particle sizes was undertaken to examine whether the glasses crystallized via bulk or surface nucleation. Frit, coarse, and fine fraction powders were examined in the DSC at a heating rate of  $10 \text{ K min}^{-1}$ . Since there is a significant difference in the surface:volume ratio between frit and fine fraction, any glass with surface nucleation tendencies will crystallize at a lower temperature for fine powders.

Following the method of Marrota et al. [18], the optimum nucleation temperature (ONT) of the glass was also found using DSC analysis. The ONT is defined as the temperature at which the most number of stable nuclei form per volume element. The ONT is found by heating the glass powder to temperatures between  $T_{g,\text{onset}}$  and  $T_{p1}$ , then holding for 1 h before heating the sample to above  $T_{p2}$ . Repeating this for a number of hold temperatures allows the hold temperature which produces the lowest crystallization temperature to be found. This is the ONT. In all cases, a heating rate of  $10 \text{ K min}^{-1}$  was used.

### 2.3 X-ray diffraction (XRD)

Powder XRD was performed to confirm the phases present in the samples. Prior to XRD, frit samples were crystallized by heating in the DSC furnace to ensure accurate temperature and heating rate control. Frit was used to minimise any surface effects. The samples were then crushed and sieved to  $<45 \mu\text{m}$ . Analysis was carried out in a Huber 642 Guinier Diffractometer (Rimsting, Germany) with a quartz Johansson monochromator and copper target operating in subtractive transmission mode at 40 kV and 30 mA. X-rays were pure monochromatic  $\text{Cu } K\alpha_1$  with  $\lambda = 1.54056 \text{ \AA}$ . Si powder (pure element grade, 99.5% pure, Johnson Matthey Alfa Products, Karlsruhe, Germany) was added at 10 wt% to all crystallized samples as an internal standard to allow correction for non-linear peak shift.

### 2.4 Optical microscopy

Samples were mounted in epoxy, ground with SiC paper, polished to  $<1 \mu\text{m}$  finish using a diamond paste. To image the microstructures of the metals they were etched by first using concentrated HF for 1 s, then 5 s in a solution of 10 ml KOH (40%), 5 ml  $\text{H}_2\text{O}_2$  (30%), and 20 ml  $\text{H}_2\text{O}$ . The solution dissolves the  $\beta$ -phase quicker than the  $\alpha$  phase. The samples were washed with water, alcohol and then acetone before drying. Optical imaging was carried out using a Leica MEF4M (Wetzlar, Germany).

### 2.5 Glass enamelling procedure

The coating was deposited on the substrates using a simple sedimentation route. Prior to sedimentation, the substrates

were roughened with 80 grit SiC paper, washed in water, alcohol then acetone. This was done to remove any release agents i.e., grease, oil, scale, etc and to provide extra interfacial bonding area [15]. Glass powder of  $<45 \mu\text{m}$  was mixed with ethanol to create a slurry. This was poured onto the substrate and ultrasonic agitation used for 3 min to give a homogeneous layer and break-up any powder aggregates. The sample was placed in a vacuum oven at  $120^\circ\text{C}$  for 24 h to dry. It was then heat treated in vacuo in a muffle furnace at  $10 \text{ K min}^{-1}$ .

### 2.6 Scanning electron microscopy (SEM)

Samples for electron microscope analysis were mounted, ground, and polished as for optical microscopy. They were then gold sputter-coated and analysed in a JEOL JSM 840 scanning electron microscope in both secondary electron imaging (SEI) and backscattered electron imaging (BEI) modes. Energy dispersive X-ray (EDX) spectroscopy was used to determine the elements present in some samples.

## 3 Results and discussion

### 3.1 Response of $\text{Ti}_6\text{Al}_4\text{V}$ to high temperatures

To confirm the upper limit to the temperature at which enamelling should be done, the response of  $\text{Ti}_6\text{Al}_4\text{V}$  to continuous heating was investigated. The volumetric expansion due to the allotropic transformation from  $\alpha + \beta \rightarrow \beta$  could generate internal stresses in the coating and might result in delamination. In addition, the fatigue strength of the alloy may be compromised [1]. This transformation is therefore to be avoided. A sample of  $\text{Ti}_6\text{Al}_4\text{V}$  was examined in a DSC at a heating rate of  $10 \text{ K min}^{-1}$  in a dry nitrogen atmosphere. This allows the determination of temperature dependent phase changes. Peaks were observed at 865, 1014 and  $1175^\circ\text{C}$ . These results are similar to those previously published by Sha and Guo [21] and Boivineau et al. [3]. The peak at  $865^\circ\text{C}$  corresponds to the transformation of the  $\beta$  phase to a high temperature  $\beta$  phase and the peaks at 1,014 and  $1,175^\circ\text{C}$  have been described above by Sha and Guo [21] as  $\alpha + \beta \rightarrow \beta$ .

To observe the effect of temperatures above the  $\alpha + \beta \rightarrow \beta$  transformation, two  $\text{Ti}_6\text{Al}_4\text{V}$  samples were heat treated to 1,000 and  $1,200^\circ\text{C}$  then cooled in the furnace at  $40 \text{ K min}^{-1}$  once they had reached the target temperature, see Fig. 1. The effect of the peak at  $865^\circ\text{C}$  on the microstructure was difficult to observe in the  $1,000^\circ\text{C}$  sample but the changes between 1,014 and  $1,175^\circ\text{C}$  were significant. Once the samples were heated to above the  $\alpha + \beta \rightarrow \beta$  transus, a Widmannstätten morphology formed upon

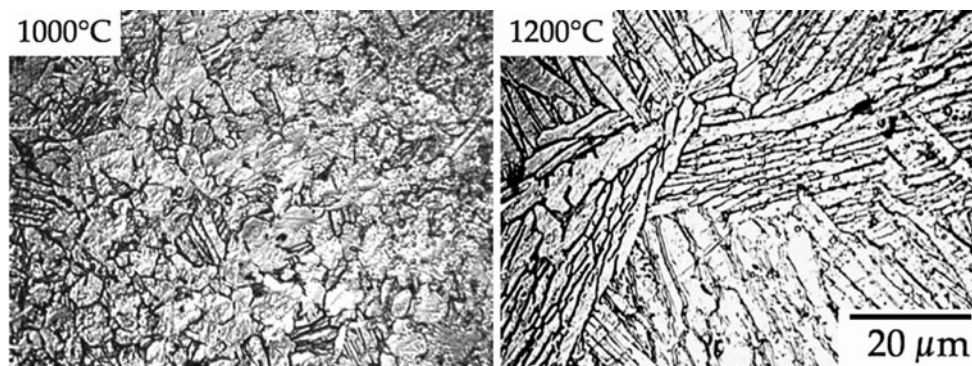


**Fig. 1** The onset of the  $\alpha + \beta \rightarrow \beta$  transformation occurs at 970°C. The microstructures of  $\text{Ti}_6\text{Al}_4\text{V}$  heat treated to 1,000 and 1,200°C are shown and the evolution of Widmannstätten is clearly seen

cooling. The Widmannstätten structure comprises plates of  $\alpha$ -phase surrounded by dark areas of  $\beta$ -phase. Figure 1 shows a sample heated to 1,000°C where the Widmannstätten structure is beginning to form but has not reached equilibrium as there was insufficient time for it to fully form. In the 1,200°C sample, the Widmannstätten has completely formed and these structures have undergone grain coarsening due to the elevated temperature.

These results imply that any glass suitable for enamelling must be devitrified below the onset temperature for Widmannstätten which is 970°C. The glass must be fully crystalline because significant levels of residual glass could adversely affect the mechanical properties of the coating.

### 3.2 Thermal analysis of glass

DSC was used to determine the thermal characteristics of the glasses. The results are tabulated in Table 2. It has been previously shown that the crystallisation exotherms correspond to the formation of apatite at  $T_{p1}$  and the interdependent co-crystallisation of apatite and mullite at  $T_{p2}$  [25].

The low and intermediate fluorine content glasses, G100, G125, G150, and G175 showed surface nucleation characteristics while the high fluorine content glasses G187, G200, G220, and G250 showed bulk nucleation characteristics. Some of the low fluorine glasses did not show a distinct  $T_{p1}$  and therefore this value was not reported for some compositions. These results would suggest that only the high fluorine content glasses be considered for coatings both because they crystallise via bulk nucleation and at temperatures below 970°C. Surface nucleation is an undesirable characteristic for enamelling since it could inhibit particle bonding.

### 3.3 Sintering and crystallization of glass powders

To examine how well each of the glass compositions sinter, disks of each glass type were pressed from <45  $\mu\text{m}$  powder

and sintered to determine if there was a difference in densification between low and high fluorine glasses. Initially, disks of each glass were heated to 1,200°C at 10  $\text{K min}^{-1}$  and then cooled. The results are shown in Fig. 2. Heating all of the samples to the same temperature allows differences resulting from the fluorine content to be examined. It would be expected that the glasses with the lowest viscosity would sinter best. These glasses should be the high fluorine glasses as the fluorine acts to increase network mobility and lower viscosity.

Surprisingly however, the images in Fig. 2 clearly show that the lower fluorine content glasses are the most sinterable. This result was unexpected for this experiment but does further validate the previously published result that glasses with higher fluorine contents also have higher activation energies for crystal growth of the FAp phase [19]. With higher F contents comes higher nucleation densities and a concomitant localised depletion of fluorine, phosphorous and calcium around the nascent crystals. This in turn gives higher network connectivity in the residual glassy matrix which gives a higher activation energy for growth due to kinetic hindrance. This same mechanism is likely to inhibit inter-particle bonding of the glassy phase.

It could also be that the crystallization of mullite at lower temperatures in the high fluorine glasses inhibits particle bonding since mullite is a high temperature refractory ceramic and would be quite stable at high temperatures. The presence of mullite therefore hinders densification. The low fluorine glasses have a delayed mullite crystallization onset temperature that allows the temperature of the pressed disks to be raised sufficiently high for particle necking and bonding to occur before the mullite crystallizes.

A third possibility is related to the temperature difference between  $T_{p1}$  and  $T_g$ ; lower fluorine glasses have a greater difference between  $T_g$  and  $T_{p1}$  which could allow the glass to flow and densify better prior to the crystallization of FAp. These latter mechanisms can be considered

**Table 2** Summary of results from DSC study of the glasses. All results are from runs done at 10 K min<sup>-1</sup>

Glass code	G250	G220	G200	G187	G175	G150	G125	G100
Firing temp (°C)	1420	1420	1420	1430	1430	1440	1440	1440
$T_{g,mid}$	629	634	650	663	676	696	709	726
$T_{p1}$								
Frit	694	743	754	791	837	918	1011	1040
Coarse	686	738	751	792	822	923	–	–
Fine	686	741	755	797	821	917	926	–
$T_{p2}$								
Frit	838	907	964	991	1033	1074	1102	1123
Coarse	835	911	968	999	1006	1003	1047	1061
Fine	839	908	959	989	999	1018	1025	1033

Some of the low fluorine glasses did not show a distinct  $T_{p1}$  and therefore this value was not reported for some compositions

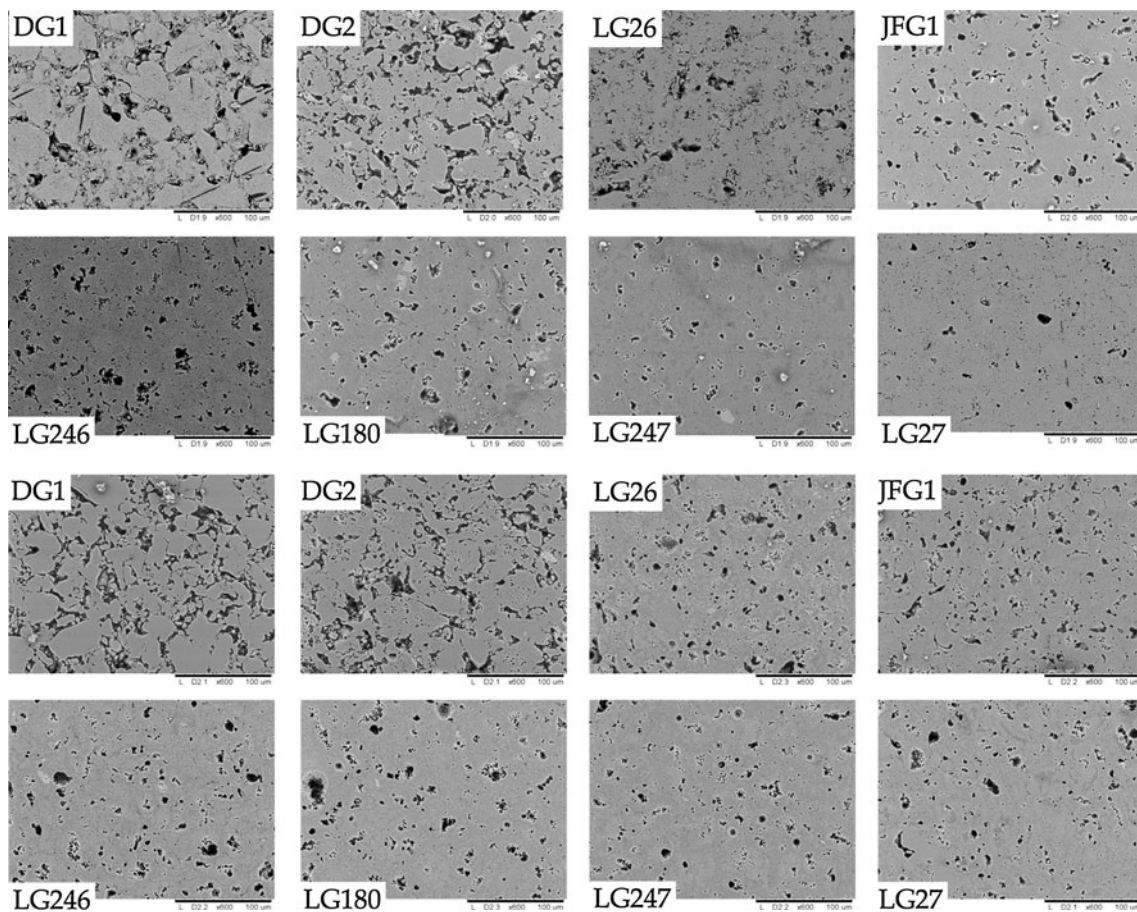


**Fig. 2** SEM images of pressed and sintered disks of each glass. The *upper half* shows samples heated to their respective  $T_{p2, end}$ . The *lower half* shows samples heated to 1,200°C. Surprisingly the high fluorine content glasses sintered poorly in both cases

in themselves to be outcomes of the initial explanation given above pertaining to effects of fluorine content on ease of nucleation in the respective glasses and the effects that this then has on phase evolution. A final possibility worthy of note is that SiF<sub>4</sub> evolution from the surface of the high fluorine glasses is causing anorthite (CaAl<sub>2</sub>Si<sub>2</sub>O<sub>8</sub>) to

be formed on the surface and this is preventing densification. This, however, is unlikely as the glass system is designed to limit the amount of SiF<sub>4</sub> loss.

A second heat treatment regime was also examined where the powder disks were heated at 10 K min<sup>-1</sup> to their respective  $T_{p2, end}$  then cooled, see Fig. 2. This was done to

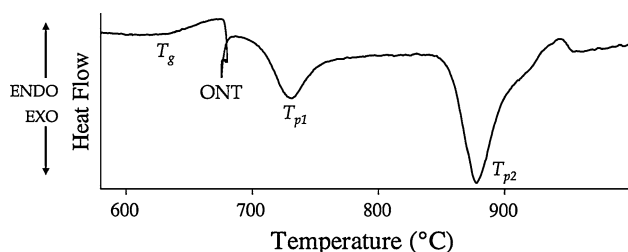


**Fig. 3** DSC of G200 heated at  $10 \text{ K min}^{-1}$  and held at its ONT of  $670^\circ\text{C}$  for 60 min then heated to above  $T_{p2,\text{end}}$

examine the resultant densification when each powder disc was heated to a temperature just sufficient to cause complete crystallization. The densification results show the same trend seen in previous samples.

There appears to be little difference in the density of G100 to G200 as compared with the relatively poor densification of G220 and G250 which exhibited very little particle bonding. G200 was therefore chosen as the most suitable of the “sinterable” glasses for enamelling as it has a low crystallisation temperature and will crystallise below the Ti transus.

The process of bond formation between particles may be simplified to give the following expression of the change in particle volume,  $V$ , as a function of time,  $t$ , and absolute temperature,  $T$  [14]:

$$\frac{\Delta V}{V_0} \propto \left(\frac{t}{T}\right)^{2/5} \quad (1)$$

This equation predicts that higher sintering temperatures will require a shorter time to achieve densification. It has been shown for a number of metal and ceramic systems that the shrinkage of a powder compact proceeds at a rate proportional to  $t^{2/5}$  [14]. This relationship is also qualitatively seen here in the densification of the coatings where lower temperature coatings require a longer time to densify.

#### 3.4 Effect of heat treatment hold time and temperature on coating morphology

Since G200 was chosen as the most suitable glass, it is useful to see in more detail the thermal characteristics of G200 heated at  $10 \text{ K min}^{-1}$  and held at its ONT of  $670^\circ\text{C}$  for 60 min then heated to above  $T_{p2}$ , as shown in Fig. 3. Comparing this figure to the DSC graph of  $\text{Ti}_6\text{Al}_4\text{V}$  in Fig. 1, it can be seen that G200 will be fully crystallized before the  $\text{Ti}_6\text{Al}_4\text{V } \alpha + \beta \rightarrow \beta$  transformation onset occurs at  $970^\circ\text{C}$ .

To enamel G200 to the roughened substrate (produced by P80 SiC paper to give a substrate  $R_a$  of  $1,380 \mu\text{m}$ ), the samples of sedimented G200 on  $\text{Ti}_6\text{Al}_4\text{V}$  were heated at  $10 \text{ K min}^{-1}$  to the G200 ONT and held isothermally for 1 h, then heated and held at different times and temperatures

at or above  $T_{p2,\text{end}}$ . This elucidates the effect of different time–temperature combinations on the resulting coating morphology and substrate microstructure. The heat-treatment profile is designed to fully crystallize the glass–ceramic, since it is above the  $T_{p2,\text{end}}$  for G200, and also to adhere it to the substrate without heating above the  $\text{Ti}_6\text{Al}_4\text{V } \alpha + \beta \rightarrow \beta$  transition ( $970^\circ\text{C}$ ) as this could affect the fatigue properties of the metal [1]. The samples were allowed to cool slowly in the furnace to prevent the coatings from cracking due to differential cooling rates between coating and substrate. The glass composition chosen has a thermal expansion coefficient similar to that of  $\text{Ti}_6\text{Al}_4\text{V}$  [23] so delamination should not occur if the coating is well adhered.

The resultant coatings are shown in Fig. 4. It shows that AMGCs can be successfully enamelled to  $\text{Ti}_6\text{Al}_4\text{V}$  under a number of different processing conditions. Three broad groups of coatings have been defined: under-sintered, optimally-sintered, and over-sintered. Under-sintered coating coatings are characterised by a lack of particle cohesion that would result in a friable coating. Over-sintered coatings had a very closed coating morphology and inspection of the interface showed that excessive interfacial reactions occurred, as evinced by the non-planar surface of the substrate (see Sect. 3.5). Optimally sintered coatings had a relatively planar substrate surface and a reasonably open coating morphology that should encourage mechanical fixation of bone onto it [2, 7]. It is acknowledged that the pores present are not large enough to facilitate bone ingrowth [9] where channels of  $> 110 \mu\text{m}$  are required.

The most suitable coating was determined to be the sample sintered at  $940^\circ\text{C}$  for 30 min, called the “optimised” sample. This sample has been heated to a temperature just sufficient to cause full crystallization of the glass. Full crystallization is required to improve the bio-activity of the glass [8] and this is the lowest possible temperature at which this occurs for this glass. This relatively low temperature reduces the degree of grain growth in the substrate and removes the risk of Widmannstätten forming. The coating has numerous “bowl-like nests” as suggested by Bigerelle et al. [2] and has a rougher coating than the over-sintered coatings, which should enhance cell proliferation [7]. Having a slower formation of the coating allows for greater control over the exact resultant coating, for example at  $1,000^\circ\text{C}$  the optimal coating forms very quickly and may be difficult to control.

The corresponding microstructure of the substrate resulting from each of the sintering routes was also examined and these are shown in Fig. 5. There is some grain growth evident in the substrate when heat-treated under the “optimal” regime and an overall loss in the rolling texture evident even at the lowest time and temperature combination.

**Fig. 4** The resultant coating morphologies from a variety of heat treatment profiles

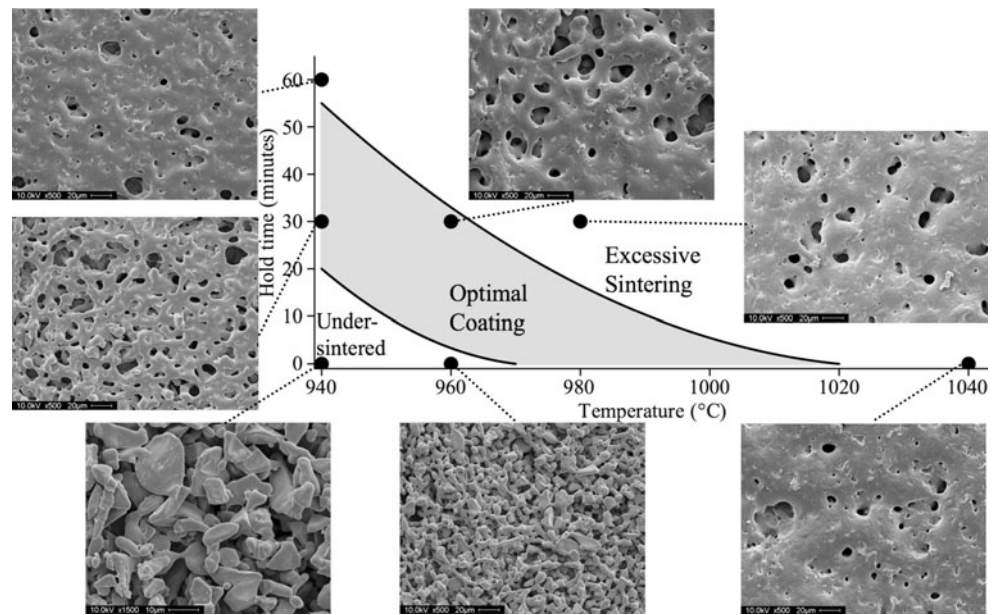
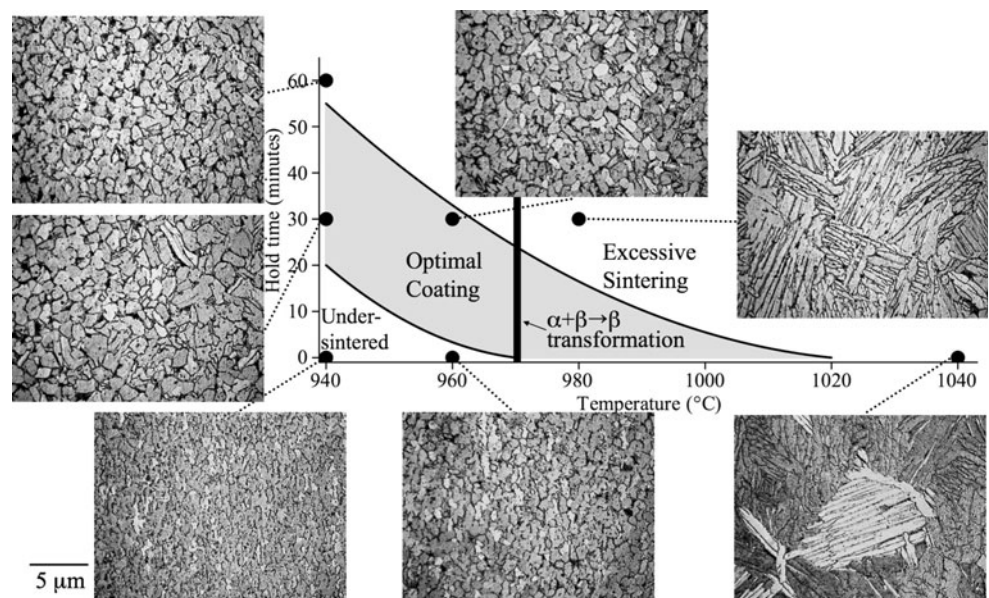


**Fig. 5** Microstructures of the substrates corresponding to the different coating morphologies produced in Fig. 4. The different AMGC coating regions discussed in Fig. 4 are identified for reference



### 3.5 Analysis of coating–substrate interface

The nature of the coating–substrate interface formed during the optimised sintering route was examined by inspecting a cross-section from an optimised sample. The AMGC appears to be well bonded to the  $Ti_6Al_4V$ , with no cracking evident in the coating. The substrate interface is largely planar indicating that an excessive reaction did not take place, see Fig. 6. Backscattered electron imaging (BEI-SEM) shows that there are three regions in the interface—the titanium alloy substrate on the left which is bright due to the relatively high atomic number of Ti, an interfacial region, and the homogeneous apatite–mullite coating, see Fig. 6. EDX across the interface shows that the region is

formed with Ti, Si, Ca, and P, similar to previously examined interfaces [25].

To test the adhesion of the coating, the relative crack resistance was qualitatively determined using Vickers microindentation on the interface between the substrate and coating. Indentations were made on the polished cross section of the metal–coating interface. The crack path provides a qualitative assessment of the adhesion at this interface. Vickers indentation on the interface has been previously used to qualitatively determine bond strength by Gomez-Vega et al. [11] and Lopez-Esteban et al. [17]. However, it is recognised that a more comprehensive investigation is needed due to the complex nature of the loading in vivo and detailed mechanical testing will be

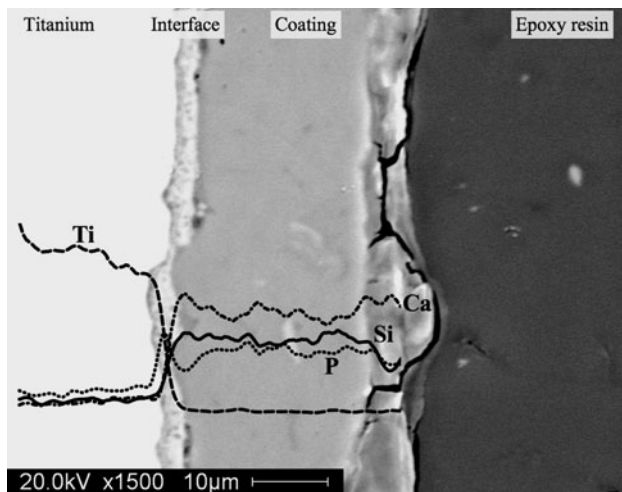


**Fig. 6** BEI-SEM of the optimised heat treatment route substrate-coating interface between G200 and  $\text{Ti}_6\text{Al}_4\text{V}$ . An EDX line scan was used to examine the variation in elements across the interface

carried out in a separate study. To demonstrate the influence of the reaction zone on the mechanical properties, an ‘oversintered’ sample with an excessively large reaction zone was chosen. This should elucidate the crack/material interaction clearer than a sample with a smaller zone. After indentation, the cracks did not propagate along the reaction region interface but instead tend into the coating. This indicates that the reaction interface is well adhered to both the substrate and the coating: see Fig. 7. Residual interfacial stress is assumed to not play a significant role in crack development here as the sample is well-annealed and crack did not travel very far.

### 3.6 Effect of heat treatment on oxygen infiltration

Oxygen is an  $\alpha$ -stabiliser in titanium, forming  $\alpha$ -case when it diffuses from the atmosphere into the alloy. This can have negative effects on the fatigue properties of the substrate as it can embrittle the alloy, commonly known as *oxygen embrittlement*. To quantify the depth of oxygen infiltration—even though samples here are heat treated in vacuo—a  $\beta$ -titanium alloy known as TMZF ( $\text{TiMo}_{12}\text{Zr}_6\text{Fe}_2$ , [28]) was heated and held at two different hold times and temperatures. Oxygen diffuses into the  $\beta$ -alloy grain boundaries and into grains along preferential crystallographic directions and thereby stabilises the  $\alpha$  phase. The  $\alpha$ -phase can then be preferentially etched to reveal the diffusion paths.

Samples of TMZF were subjected to the previously published AMGC enamelling route<sup>1</sup> and to an “optimised”

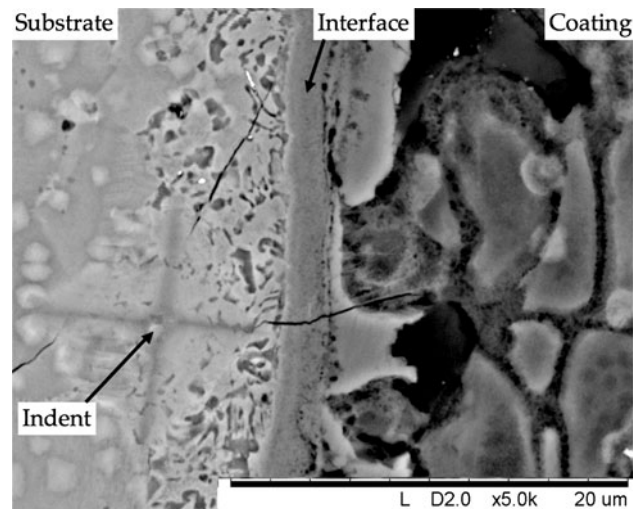


**Fig. 7** Indentation testing of the bond strength of the coating. There appears to be good adhesion between the layers, as the cracks tended toward the homogeneous coating. The coating has a granular structure with grains of AMGC bonded together

heat treatment schedule, both under vacuum, for comparison. In the case of the optimised route, the sample was heated at  $10 \text{ K min}^{-1}$  to  $640^\circ\text{C}$  (the ONT for G200) and held for 60 min, then heated then to  $940^\circ\text{C}$  for 30 min then cooled at  $10 \text{ K min}^{-1}$ . The sample cross-sections were then ground, polished, and etched as described in Sect. 2.4. The distance into the substrate that the oxygen diffused was measured at a number of different locations using optical microscopy and the average distance was found.

The results show that the optimised route results in significantly less oxygen infiltration to the substrate, with a reduction of almost 63%, see Fig. 8. The average diffusion depth for sample (a) was  $25.7 \mu\text{m}$  ( $\pm 4.8$  standard deviation) and  $9.6 \mu\text{m}$  ( $\pm 4.4$  standard deviation) for sample (b). Visually there is also a clear difference between the samples, see Fig. 8a for the original route, Fig. 8b shows the optimised route results and Fig. 8c shows the normal grain structure of TMZF.

Oxygen embrittlement of titanium and titanium alloys, i.e. the formation of alpha case in  $\text{Ti}_6\text{Al}_4\text{V}$ , is severely detrimental to the fatigue properties of the metal and the new optimised route shows that the level of oxygen diffusion and hence embrittlement can thus be significantly reduced.

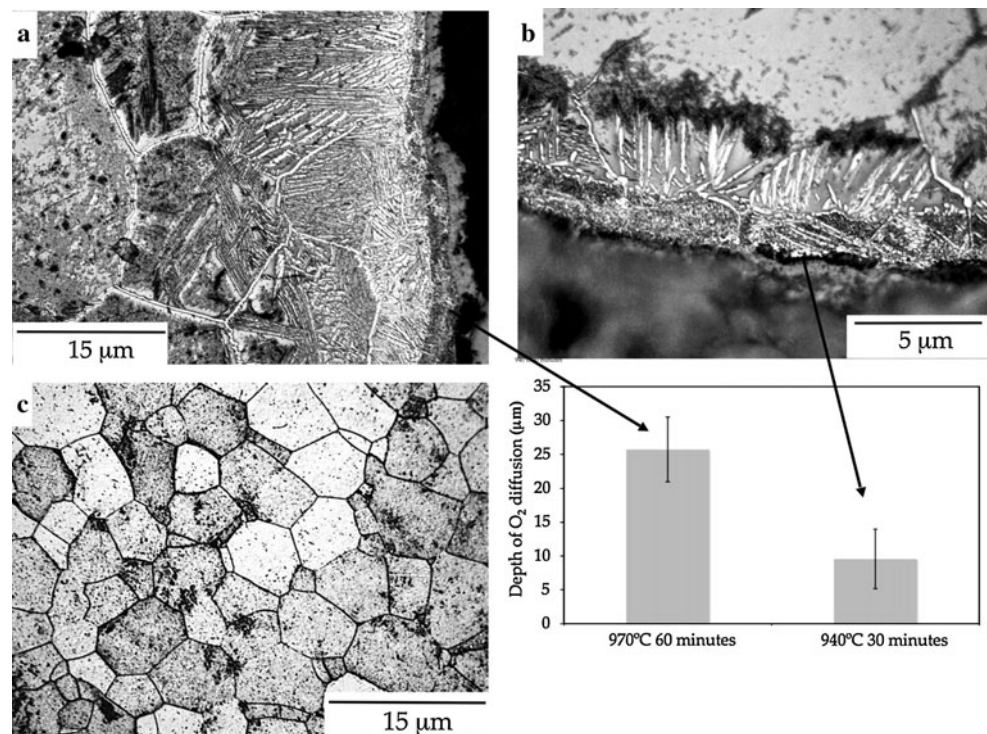
<sup>1</sup> Stanton and Vanhumbecck [23] first described a successful route for enamelling AMGC to  $\text{Ti}_6\text{Al}_4\text{V}$ . The following protocol was used: G187 was sedimented on  $\text{Ti}_6\text{Al}_4\text{V}$  in the same manner as used here then heated from room temperature at  $10 \text{ K min}^{-1}$  to  $670^\circ\text{C}$  (the

Footnote 1 continued

ONT for G187 [23]); held for 60 min;  $670\text{--}960^\circ\text{C}$  at  $10 \text{ K min}^{-1}$ ; held for 90 min; cool to ambient at  $10 \text{ K min}^{-1}$ .



**Fig. 8** Etched samples of TMZF. The top two have been heat-treated according to **a** the previously published enamelling route [23], and **b** the new optimised route. The oxygen diffusion paths are clearly evident. Sample **c** is a normalised sample of TMZF for comparison. The grain size of sample **a** has also increased when compared to the grain size for the normalised sample. The oxygen penetration depth into TMZF for the two different heat treatment profiles is graphed. The *error bars* show the standard deviation of the measurements



#### 4 Conclusions

AMGC coatings on Ti<sub>6</sub>Al<sub>4</sub>V were investigated to determine an improved heat treatment regime using a systematic examination of the different inputs: composition of glass, nucleation hold and crystallisation hold.

DSC analysis of the titanium alloy (Ti<sub>6</sub>Al<sub>4</sub>V) shows that the  $\alpha + \beta \rightarrow \beta$  transformation occurs at around 970°C. Above that temperature, Widmannstätten form which are detrimental to the fatigue properties of the substrate. This sets a maximum heat treatment temperature. A suitable glass must therefore crystallise and adhere to the substrate below this temperature.

DSC analysis of the glasses identified a transition from surface to volume nucleation of the glass as the fluorine content increases. Surface nucleation is to be avoided as the glass needs to be homogeneously crystallised. A powder sintering study showed however that lower fluorine glasses densify better. It is postulated that this occurs because of their lower nucleation density giving a lower overall network connectivity in the residual glassy phase [19].

G200 was chosen as the most suitable glass as it was the best compromise between high enough fluorine to crystallise fully at temperature below the  $\alpha + \beta \rightarrow \beta$  transition for Ti<sub>6</sub>Al<sub>4</sub>V but a low enough fluorine content to densify sufficiently.

Samples of G200 sedimented on Ti<sub>6</sub>Al<sub>4</sub>V were heated to a number of time–temperature combinations above  $T_{p2,end}$  and the subsequent coating morphology was examined.

‘Under-sintered’ coatings remained friable and had poor particle cohesion. ‘Over-sintered’ coatings had a very closed coating morphology and inspection of the interface showed that excessive interfacial reactions occurred. ‘Optimally sintered’ coatings had a relatively planar substrate surface and a reasonably open coating morphology that is tough to encourage mechanical fixation of bone onto it.

The Ti<sub>6</sub>Al<sub>4</sub>V substrate microstructure for most of the coatings showed some grain growth and this was attributed to recrystallisation of the metal grains at elevated temperatures during the heat treatment process. Coatings that were sintered above the  $\alpha + \beta \rightarrow \beta$  transition showed a Widmannstätten type microstructure.

EDX analysis of the G200–Ti<sub>6</sub>Al<sub>4</sub>V interface indicated that some diffusion of elements across the boundary did occur and a reaction interface formed. Indentation testing of the qualitative strength of the coating showed that there was good adhesion between the coating and the substrate and the interfacial layer did not cause crack propagation.

An examination of the depth to which oxygen diffused into the substrate during heat treatment was done using TMZF. Results show that there was a reduction of almost 63% between the previously published initial results and the present optimised route.

**Acknowledgements** Part funding was provided by the Irish Research Council for Science, Engineering and Technology: funded by the National Development Plan. The authors also acknowledge the support from the UCD Nano Imaging and Material Analysis Centre (NIMAC) funded by Science Foundation Ireland (SFI).

## References

- Akahori T, Niinomi M, Fukunaga K, Inagaki I. Effects of microstructure on the short fatigue crack initiation and propagation characteristics of biomedical  $\alpha/\beta$  titanium alloys. *Metall Mater Trans A*. 2000;31A(8):1949–1958.
- Bigerelle M, Anselme K, Nol B, Ruderman I, Hardouin P, Iost A. Improvement in the morphology of Ti-based surfaces: a new process to increase in vitro human osteoblast response. *Biomaterials*. 2002;23(7):1563–1577.
- Boivineau M, Cagran C, Doytier D, Eyraud V, Nadal M, Wilthan B, Pottlacher G. Thermophysical properties of solid and liquid Ti–6Al–4V (TA6V) alloy. *Int J Thermophys*. 2006;27(2):507–529.
- Bowen R. Adhesive bonding of various materials to hard tooth tissues IV. Bonding to dentin, enamel, and fluorapatite improved by the use of a surface-active comonomer. *J Dent Res*. 1965;44(5):906–911.
- Clifford A, Hill R. Apatite–mullite glass–ceramics. *J Non-cryst Solids*. 1996;196(1–3):346–351.
- Cross M, Parish E. A hydroxyapatite-coated total knee replacement PROSPECTIVE ANALYSIS OF 1000 PATIENTS. *J Bone Joint Surg Br*. 2005;87(8):1073–1076.
- Deligianni DD, Katsala ND, Koutsoukos PG, Missirlis YF. Effect of surface roughness of hydroxyapatite on human bone marrow cell adhesion, proliferation, differentiation and detachment strength. *Biomaterials*. 2001;22(1):87–96.
- Freeman C, Brooks I, Johnson A, Hatton P, Hill R, Stanton K. Crystallization modifies osteoconductivity in an apatite–mullite glass–ceramic. *J Mater Sci Mater Med*. 2003;14:985–990.
- Frosch K, Barvencik F, Viereck V, Lohmann C, Dresing K, Breme J, Brunner E, Sturmer K. Growth behavior, matrix production, and gene expression of human osteoblasts in defined cylindrical titanium channels. *J Biomed Mater Res A*. 2004;68A(2):325–334.
- Gomez-Vega J, Saiz E, Tomsia A. Glass-based coatings for titanium implant alloys. *J Biomed Mater Res*. 1999;46(4):549–559.
- Gomez-Vega J, Saiz E, Tomsia A, Marshall G, Marshall S. Bioactive glass coatings with hydroxyapatite and bioglass particles on Ti-based implants I. Processing. *Biomaterials*. 2000;21(2):105–111.
- Haverty D, Tofail S, Stanton K, McMonagle J. Structure and stability of hydroxyapatite: density functional calculation and Rietveld analysis. *Phys Rev B*. 2005;71(9):94–103.
- Kasuga T, Nogami M, Niinomi M. Preparation of calcium phosphate glass–ceramics and their coating on titanium alloys. *Key Eng Mater*. 2001;192–195:223–226.
- Kingery W, Bowen H, Uhlmann D. Introduction to ceramics (ed.). New York: Wiley; 1976.
- Kinloch A. Adhesion and adhesives. London: Chapman and Hall; 1987.
- Long M, Rack H. Titanium alloys in total joint replacement—a materials science perspective. *Biomaterials*. 1998;19(18):1621–1639.
- Lopez-Esteban S, Saiz E, Fujino S, Oku T, Sukanuma K, Tomsia A. Bioactive glass coatings for orthopedic metallic implants. *J Eur Ceram Soc*. 2003;23(15):2921–2930.
- Marotta A, Buri A, Branda F. Nucleation in glass and differential thermal analysis. *J Mater Sci*. 1981;16(2):341–344.
- O’Flynn K, Stanton K. Nucleation and early stage crystallization of fluorapatite in apatite–mullite glass–ceramics. *Cryst Growth Des*. 2010;10(3):1111–1117.
- Park D, Della Valle C, Quigley L, Moric M, Rosenberg A, Galante J. Revision of the acetabular component without cement. A concise follow-up, at twenty to twenty-four years, of a previous report. *J Bone Joint Surg*. 2009;91(2):350–355.
- Sha W, Guo Z. Phase evolution of Ti–6Al–4V during continuous heating. *J Alloys Compd*. 1999;290(1–2):3–7.
- Stanton K, Hill R. The role of fluorine in the devitrification of SiO<sub>2</sub>–Al<sub>2</sub>O<sub>3</sub>–P<sub>2</sub>O<sub>5</sub>–CaO–CaF<sub>2</sub> glasses. *J Mater Sci*. 2000;35:1–6.
- Stanton K, Vanhumbecck J. Bioactive apatite–mullite glass–ceramic coatings on titanium substrates. *Adv Sci Technol*. 2006;45:1275–1280.
- Stanton K, O’Flynn K, Newcombe S. TEM study of the reaction interface between an apatite–mullite glass–ceramic and Ti<sub>6</sub>Al<sub>4</sub>V. *Key Eng Mater*. 2007;361–363:269–272.
- Stanton K, O’Flynn K, Nakahara S, Vanhumbecck J, Delucca J, Hooghan B. Study of the interfacial reactions between a bioactive apatite–mullite glass–ceramic coating and titanium substrates using high angle annular dark field transmission electron microscopy. *J Mater Sci Mater Med*. 2009;20(4):851–857.
- Stanton K, O’Flynn K, Kiernan S, Menuge J, Hill R. Spherulitic crystallization of apatite–mullite glass–ceramics: mechanisms of formation and implications for fracture properties. *J Non-cryst Solids*. 2010;356(35–36):1802–1813.
- Tai C, Cross M. Five-to 12-year follow-up of a hydroxyapatite-coated, cementless total knee replacement in young, active patients. *J Bone Joint Surg Br*. 2006;88(9):1158–1163.
- Trentani L, Pelillo F, Pavesi F, Ceciliani L, Cetta G, Forlino A. Evaluation of the TiMo<sub>12</sub>Zr<sub>6</sub>Fe<sub>2</sub> alloy for orthopaedic implants: in vitro biocompatibility study by using primary human fibroblasts and osteoblasts. *Biomaterials*. 2002;23(14):2863–2869.